Article:
Laurent, H, Baker, DL, Soper, AK et al. (2021) Bridging Structure, Dynamics, and Thermodynamics: An Example Study on Aqueous Potassium Halides. The Journal of Physical Chemistry B, 125 (46). pp. 12774-12786. ISSN: 1520-6106

https://doi.org/10.1021/acs.jpcb.1c06728

THE JOURNAL OF PHYSICAL CHEMISTRY B
A JOURNAL OF THE AMERICAN CHEMICAL SOCIETY

pubs.acs.org/JPCB

Article

Bridging Structure, Dynamics, and Thermodynamics: An Example Study on Aqueous Potassium Halides

Harrison Laurent, Daniel L. Baker, Alan K. Soper, Michael E. Ries, and Lorna Dougan*

Cite This: *J. Phys. Chem. B* 2021, 125, 12774–12786

Read Online

ACCESS | Metrics & More | Article Recommendations | Supporting Information

ABSTRACT: Aqueous salt systems are ubiquitous in all areas of life. The ions in these solutions impose important structural and dynamic perturbations to water. In this study, we employ a combined neutron scattering, nuclear magnetic resonance, and computational modeling approach to deconstruct ion-specific perturbations to water structure and dynamics and shed light on the molecular origins of bulk thermodynamic properties of the solutions. Our approach uses the atomistic scale resolution offered to us by neutron scattering and computational modeling to investigate how the properties of particular short-ranged microenvironments within aqueous systems can be related to bulk properties of the system. We find that by considering only the water molecules in the first hydration shell of the ions that the enthalpy of hydration can be determined. We also quantify the range over which ions perturb water structure by calculating the average enthalpic interaction between a central halide anion and the surrounding water molecules as a function of distance and find that the favorable anion−water enthalpic interactions only extend to ∼4 Å. We further validate this by showing that ions induce structure in their solvating water molecules by examining the distribution of dipole angles in the first hydration shell of the ions but that this perturbation does not extend into the bulk water. We then use these structural findings to justify mathematical models that allow us to examine perturbations to rotational and diffusive dynamics in the first hydration shell around the potassium halide ions from NMR measurements. This shows that as one moves down the halide series from fluorine to iodine, and ionic charge density is therefore reduced, that the enthalpy of hydration becomes less negative. The first hydration shell also becomes less well structured, and rotational and diffusive motions of the hydrating water molecules are increased. This reduction in structure and increase in dynamics are likely the origin of the previously observed increased entropy of hydration as one moves down the halide series. These results also suggest that simple monovalent potassium halide ions induce mostly local perturbations to water structure and dynamics.

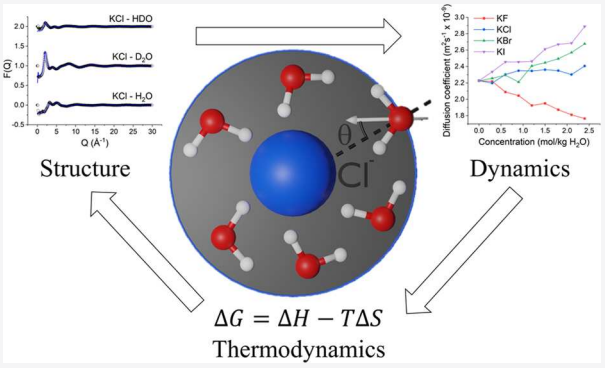

INTRODUCTION

The interactions between water and ions play a vital role in life across multiple length scales.[1−5] At the molecular level, the delicate interplay between ion−water interactions and ion−biomolecule interactions results in perturbations to biomolecular stability fundamental to life as we know it.[6−9] At the mesoscale, ion−water interactions play a key role in the manufacturing of food,[10] textiles,[11] and the mining industry.[12] Finally, at the macroscale, understanding the ion−water interactions present in clays can help us to understand and prepare for environmental processes such as mudslides[13] and also understand the properties of recently discovered extraterrestrial bodies of liquid water.[14−17]

An important and long-standing question that applies to all of these fields concerns the distance over which ions perturb water structure and dynamics.[18−22] These perturbations principally occur as a result of a balance between favorable electrostatic interactions between the charged ion and the local partial charges present on the water molecule (hydrophilic), as well as the excluded volume and network reshaping as a result of inserting the ion into the water network (hydrophobic).[5] The nature of these interactions means that small highly charged ions exhibit a more hydrophilic character than larger more weakly charged ions; however, both require substantial water network reorganization, and therefore perturbations to water−water hydrogen bonding, to incorporate the ions.

The work of Hofmeister in the 1880s showed that different ionic species can affect the stability of biomolecules such as proteins to different extents,[23−26] resulting in a ranking of ions from stabilizing agents, or kosmotropes, to destabilizing agents, or chaotropes. The previously accepted view was that the origin of this effect was due to long-ranged effects of the ions

Received: July 29, 2021
Revised: October 15, 2021
Published: November 10, 2021

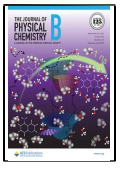

https://doi.org/10.1021/acs.jpcb.1c06728
J. Phys. Chem. B 2021, 125, 12774−12786

on water structure.[3,27,28] Kosmotropes were suggested to enhance water structure, and therefore increase protein stability, and chaotropes were suggested to destroy water structure and hence reduce protein stability.[22,27,29] However, recent studies from spectroscopic, scattering, and simulation techniques[3,22] have demonstrated that the effects of several ion species on water are limited to the first few hydration shells (~5 Å) and do not extend into the bulk solution. This is particularly true for simple monovalent ions, such as those discussed in this work; however, divalent and polyatomic ions, such as Mg^{2+} and ClO_4^-, have been shown to induce more global changes to water structure at high concentrations (44 wt %) in a similar manner to large external pressures.[30] The ability of particular ion species to act as a protein is therefore thought to be due to local interactions between ions and the protein surface.

Neutron scattering studies allow for the determination of site-specific radial distribution functions (RDFs), which allow changes in the solute−water and water−water correlations to be monitored. These studies have shown that water forms two- to three-ordered hydration shells around ions, corresponding to a distance of ~5 Å,[30−33] suggesting that short-range perturbations are relevant. Studies of ions in solution from X-ray[34,35] scattering, nuclear magnetic resonance (NMR),[1,2,36] dielectric spectroscopy,[22,37,38] infrared spectroscopy techniques,[39,40] simulations, and modeling[25,41,42] also suggest short-ranged effects over similar length scales (~5 Å).

In this study, we choose to investigate aqueous potassium halides and employ a novel combination of neutron diffraction with computational modeling and NMR to obtain a detailed structural and dynamic analysis of the effects of monovalent ions in solution. The combined study attempts to bridge the gap between atomistic level information and bulk ensemble information. This is done by studying specific microenvironments present in aqueous potassium halide solutions and testing whether the properties of these microenvironments can be extrapolated to capture experimentally observable bulk thermodynamic properties. As measurable thermodynamic properties of aqueous systems originate from both structural and dynamic perturbations to water, it is crucial that both perturbations are monitored. Neutron scattering and computational modeling are used to study the structural perturbations to water present in the microenvironments of interest; however, this method is incapable of monitoring dynamic perturbations. Hence, NMR is used as a complimentary experimental technique to study the dynamic perturbations to water present in the microenvironments of interest and complete the microscale picture of aqueous potassium halides. This novel combination of the two techniques allows us to highlight the structural and dynamic perturbations that result in the observed thermodynamics of hydration of potassium halides.

Halides are those elements that belong to group 7 of the periodic table, including fluorine, chlorine, bromine, and iodine. These were chosen as they are simple monovalent ions with large biological relevance[43,44] for which neutron scattering data is already available.[32] We observe that structural perturbations are almost entirely limited to the first hydration shell of the ion and that these interactions can account for bulk experimental measurements such as the enthalpy of hydration. We then go on to use this observation as the foundation for mathematical modeling, which allows us to quantify the perturbations to rotational and diffusive dynamics of water molecules in the first hydration shells of potassium halide ions from NMR data. Finally, we consider the results for both structural and dynamic perturbations to the hydrating water molecules induced by the ions and comment on the entropy of hydration for each salt.

MATERIALS AND METHODS

Neutron Diffraction. Neutron diffraction data on the aqueous potassium halides KF, KCl, KBr, and KI at 0.6, 1.2, and 2.4 mol/kg H_2O in H_2O, D_2O, and HDO was taken from the previous work of Soper and Weckström.[32] These concentrations are of biological relevance. For example, the intracellular concentration of K^+ is 0.14 M and of Cl^- is 0.25 M[45] and the concentration of saturated KCl is 4.8 mol/kg H_2O at 25 °C.[46] Original data was taken at the ISIS neutron and muon source on the Small Angle Neutron Diffractometer for Amorphous and Liquid Samples (SANDALS) instrument using TiZr cans normalized to a vanadium standard. Data was corrected for multiple scattering, attenuation, and inelasticity effects using Gudrun.[47]

Empirical Potential Structure Refinement (EPSR). The data was analyzed using the Monte Carlo-based structural refinement technique, empirical potential structure refinement (EPSR).[48,49] This first builds a simulated box of atoms and molecules at the same concentration and density as the experimental sample. Each atom present in the sample is characterized by a reference potential consisting of a charge q and the Lennard-Jones parameters σ and ϵ using the standard Lorentz−Berthelot mixing rules (see Table S1 for numerical values for each atomic species present in the simulations adopted from Soper and Weckström[32]). Water molecules are modeled using the SPC/E potential, which has been shown to accurately model dynamics and structure[50] and has been previously used in a host of EPSR studies on aqueous solutions.[6,30,32,33,51−55] To remain consistent with the previous neutron scattering and EPSR study of aqueous potassium halides of Soper and Weckström,[32] the ions were modeled using the same reference potentials as the original study. The simulations contain 5000 water molecules, and the concentration of ions is varied by introducing 60, 120, or 240 ion pairs for each of the three studied concentrations.

The simulation is then equilibrated through a Monte Carlo procedure using this reference potential for several hundred iterations to allow the simulation to reach a physically reasonable starting point. This is deemed to have occurred when the quality of the fit between the simulated and supplied diffraction data no longer changes appreciably as the simulation proceeds. Once this is complete, a further empirical potential is applied, which takes the form of a series of Poisson functions and is derived from the difference between the predicted scattering data from the simulation and the experimentally supplied scattering data.[56] The simulation then evolves further through automated modifications to the empirical potential until a satisfactory agreement exists between the simulation and the supplied scattering data. The quality of the agreement can be determined by comparing the simulated and supplied diffraction data. The result is a simulated box of atoms whose structure is consistent with the supplied scattering data, which can then be used to calculate radial distribution functions (RDFs) by accumulating >1000 iterations.

This approach has been previously employed to study various liquid systems, including aqueous amino acids,[57] ionic

https://doi.org/10.1021/acs.jpcb.1c06728
J. Phys. Chem. B 2021, 125, 12774−12786

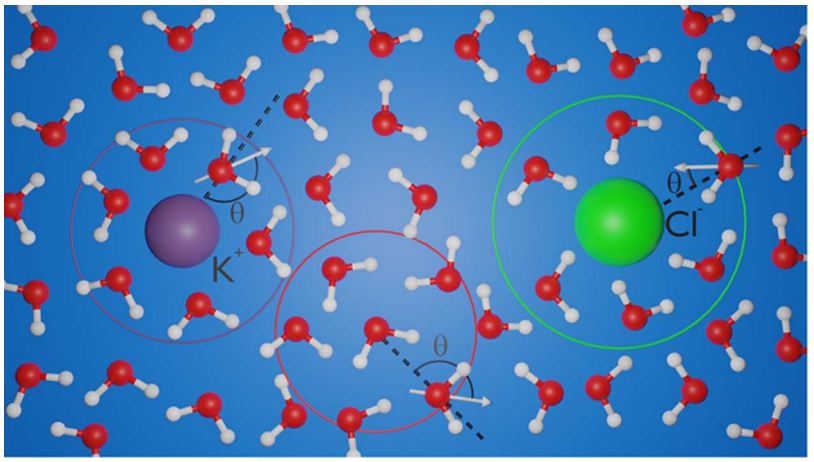

Figure 1. Schematic representation of an example potassium halide solution containing a potassium ion (purple sphere), a chloride ion (green sphere), and water molecules (red and white spheres). The first hydration shell around each ion, as well as an example for a water molecule, is shown in the color corresponding to the central atom species. The definition of the dipole angle around each of the three central ion/molecule species is labeled as θ.

liquids,[58] water−alcohol mixtures,[59] and aqueous sugars.[60] RDFs show the local density of a particular atomic species as a function of distance from a central atomic species. Hydration shells around a given central atomic species therefore occur as a series of peaks. These peaks diminish in intensity with increasing distance because the liquid nature of the samples means that only short-range order is observed, rather than solid crystalline samples where long-range order is observed through a series of Bragg peaks. At large distances, the local density of a particular atomic species therefore approaches the bulk density over the whole solution, and the radial distribution function approaches unity. EPSR can also be used to calculate coordination numbers, spatial density functions and molecular clustering.[6,61−64] The nature of this procedure does not guarantee a single unique solution to the supplied scattering data, merely one that is consistent with the scattering data and based on sensible starting potentials.

Calculation of Dipole Angle Distribution, Enthalpy of Hydration, and Distance Dependence on Enthalpic Interactions between Central Ions and Surrounding Water Molecules. Building on previous studies,[51,52] we have extracted further information from the atomic coordinates produced through EPSR to distinguish between bulk water molecules and hydration water molecules and perform a detailed analysis of various microenvironments present in the aqueous potassium halide solutions. The process of EPSR produces a simulated box of atoms consistent with the experimental neutron scattering data, each of which is given a coordinate relative to the center of the box in the x, y, and z directions. Hydration water molecules are defined as those water molecules that lie within the first hydration shell of either a potassium cation or halide anion and therefore lie within the first peak of the X−O_w RDF, where X is the ionic species and O_w is the water oxygen. The cutoff distance for the first hydration shell therefore corresponds to the minimum between the first and second peaks of this RDF (see Figure S1 and Table S2 for RDFs and calculated cutoff distances). The remaining water molecules are then classified as the bulk water molecules as they are not directly hydrating a solute ion. The results that will be shown in Figure 3 and Table 2 later in this work demonstrate that this is a sensible choice for the cutoff distance between bulk and hydration water, as beyond this point, enthalpic interactions between the ion and the surrounding water molecules are negligible. Once this distinction is made, we can then calculate various geometric and energetic properties for the hydration water molecules and the bulk water molecules, such as hydrogen bond interaction energies and angles. This latest expansion allows for the calculation of several new parameters, including the total interaction energy (enthalpy ΔH) between an ion and the water molecules in its first hydration shell (by calculating the sum of the Coulomb and van der Waals interaction potentials), the interaction energy ΔH between an ion and the surrounding water molecules as a function of distance, and the dipole angle of water molecules around both a solute ion and a bulk water molecule θ. Here, the dipole angle θ is defined as the angle between the vector that points from the ion/central bulk water oxygen to the hydrating water oxygen and the vector that is parallel to the dipole moment on the hydrating water molecule, as described in Figure 1. The dipole moment is the vector that points from the area of net negative charge on a molecule/molecular group to the area of net positive charge and therefore on a water molecule that originates at the oxygen and bisects the two hydrogens. Interatomic distances and bond angles within EPSR are described by harmonic potentials; hence, the structure of each water molecule will fluctuate slightly as the simulation proceeds. This will perturb the dipole direction; hence, to account for this, the dipole vector is calculated for each individual water molecule for every iteration by considering the coordinates for each constituent atom within the molecule, such that the dipole vector is accurately described.

H^1 Nuclear Magnetic Resonance T_1 Relaxation and Diffusion Coefficient Measurements. Samples of KF, KCl, KBr, and KI were prepared from 0 to 2.4 mol/kg H_2O in 0.3 mol/kg H_2O increments using ultrapure water such that the same concentrations studied through neutron scattering are investigated, as well as additional intermediate concentrations. T_1 relaxation time and diffusion coefficient D data are taken as previously described.[52] T_1 relaxation, data taken using a Magritek Spinsolve 43 MHz NMR spectrometer via inversion recovery, occurs following a 180° pulse, which inverts the net magnetization of the spins present in the sample. The movement of molecules in solution causes the spins on

https://doi.org/10.1021/acs.jpcb.1c06728
J. Phys. Chem. B 2021, 125, 12774−12786

individual atoms to experience time-dependent local magnetic fields of frequency ω. The spectral density of the fluctuations at the Larmor frequency ω_0 and twice the Larmor frequency determines the relaxation rate. The spectral density function $J(\omega)$ is shown in eq 1. In the fast limit $(\omega\tau_c \ll 1)$ where τ_c is the rotational correlation time, approximately equal to the time it takes for the root-mean-square deflection of a molecule to be equal to 1 rad, this expression decays to $J(\omega) = 2\tau_c$. This is the case for water molecules in aqueous solution, as rotational motions are on the order of picoseconds. The relaxation rate $\frac{1}{T_1}$ is therefore proportional to $J(\omega)$, which in turn is proportional to τ_c[36,65−67]

$$J(\omega) = \frac{2\tau_c}{1 + \omega^2\tau_c^2} \tag{1}$$

Diffusion coefficient data was acquired using a Bruker Avance II 400 MHz NMR spectrometer using the principle of pulsed field gradient spin echo.[66] Here, a magnetic field gradient G is applied parallel to the large external magnetic field causing the Larmor frequency for a particular atomic spin to be dependent on its position in the z direction. Signal attenuation is then monitored as a function of the field gradient, and the diffusion coefficient is calculated using the Stejskal−Tanner expression[68] shown in eq 2, where I_G is the signal at gradient strength G, γ is the gyromagnetic ratio of the nuclei in question, in our case hydrogen, δ is the length of the gradient pulses, and Δ is the diffusion period between gradient pulses

$$I_G = I_{G=0} \exp\left[-(\gamma\delta G)^2 D\left(\Delta - \frac{\delta}{3}\right)\right] \tag{2}$$

RESULTS

Thermodynamics of Hydration for Potassium Halides. As a first step, we calculate an important thermodynamic parameter, the enthalpy of hydration of KF, KCl, KBr, and KI, by making use of structural information from the neutron diffraction data and computational modeling. The enthalpy of hydration ΔH_{solv} for an ion is defined as "the amount of heat released when a mole of the ion dissolves in a large amount of water forming an infinitely dilute solution in the process".[69] Here, we employ an analysis routine to calculate the total interaction energy between a central ion and all of the water molecules in its first hydration shell, defined by a distance corresponding to the first minima in the ion−water RDF as described previously (see Figure S1). The calculated values for the total interaction energy around a given ion species were then averaged over the whole simulation box over 30 iterations. The results for the potassium cation and the relevant halide anion were then summed to allow the salt species to be addressed as a whole. To be consistent with the definition of the enthalpy of hydration described above, the average total first shell interaction energy was calculated for each salt species at each concentration of 0.6, 1.2, and 2.4 mol/kg H_2O and the results were extrapolated to 0 concentration to approximate an infinitely dilute solution, yielding the final value of ΔH_{EPSR} (see Figure S2). The authors are unaware of any previous attempt to use the simulations generated through EPSR in this manner. These results are compared with experimental values for the Gibbs free energy of hydration ΔG_{solv} and the enthalpy of hydration ΔH_{solv}, as reported by Tissandier et al.[70] These values are calculated by taking the difference between the free energy/enthalpy of formation of the corresponding salt and that of the gas-phase ions. The resulting values are reported in Table 1. The values for the entropy of hydration multiplied by the experimental temperature $T\Delta S_{solv}$ are also included and calculated using the standard expression for Gibbs free energy, as shown in eq 3; however, this quantity is unfortunately inaccessible through EPSR for comparison

$$\Delta G = \Delta H - T\Delta S \tag{3}$$

Table 1. Free Energy of Hydration, ΔG_{solv}, Enthalpy of Hydration, ΔH_{solv}, and Entropy of Hydration Multiplied by Experimental Temperature, $T\Delta S_{solv}$, of Potassium Halides Taken from Previous Literature[70,a]

salt species	ΔG_{solv} (kJ/mol)	ΔH_{solv} (kJ/mol)	$T\Delta S_{solv}$ (kJ/mol)	ΔH_{EPSR} (kJ/mol)
KF	−780.8	−844	−63.2	−910 ± 60
KCl	−656.2	−700	−43.8	−650 ± 20
KBr	−629.4	−669	−39.6	−600 ± 20
KI	−592.1	−627	−34.9	−610 ± 60

[a]Enthalpy of hydration calculated through EPSR by considering the total enthalpic interaction between a central halide anion and all of the water molecules in its first hydration shell and the total enthalpic interaction between a central potassium cation and all of the water molecules in its first hydration shell. Reported values correspond to the values calculated by extrapolating the calculated enthalpies within EPSR at each of the three studied concentrations to 0 mol/kg H_2O such that the definition of enthalpy of hydration, requiring an infinitely diluted solution, is maintained (Figure S2). The reported uncertainties are therefore linear combinations of the calculated uncertainties on the y intercept from the linear extrapolation of the raw data presented in Figure S2.

Here, we observe that as one moves down the halide group from F^- to I^- the Gibbs free energy, enthalpy, and entropy of hydration all become less negative. This indicates that with increasing ionic radius, and therefore decreasing charge density, the introduction of the ion into water becomes less energetically and enthalpically favorable but there is also a decreased entropy penalty. The procedure outlined in the Materials and Methods section allows the experimental enthalpy of hydration to be directly compared with the enthalpy of hydration calculated through EPSR. These results demonstrate that by only considering water molecules in the first hydration shell of an ion, the enthalpy of hydration calculated through EPSR is in close agreement with the values calculated by Tissandier et al.[70] This suggests that the thermodynamics of hydration calculated for bulk solutions of aqueous potassium halides are dominated by short-ranged interactions.

However, we must pause here to discuss the slight discrepancy between the values for the enthalpy of hydration calculated through EPSR and those calculated by Tissandier et al. The values calculated through EPSR are based on the Lennard-Jones and charge parameters for each atomic species in the system (parameters given in Table S1). They therefore derive solely from the reference potential in EPSR. However, the simulation also includes the empirical potential derived from the difference between the supplied diffraction data and the predicted diffraction data from the simulation.[56] This is expressed as a series of Poisson functions, and while its total

https://doi.org/10.1021/acs.jpcb.1c06728
J. Phys. Chem. B 2021, 125, 12774−12786

amplitude can be directly controlled, its precise form evolves with each iteration. It is therefore highly nontrivial to include in a separate analysis routine. Were the empirical potential to be included in the calculation of ΔH_{EPSR}, it is likely that the calculated values would be in closer agreement with those reported by Tissandier et al. However, the general overall agreement between the two sets of values suggests that solely using the reference potential as has been done in this work can still provide useful insight into the studied aqueous systems.

The hypothesis that short-range interactions dominate the thermodynamics of hydration in aqueous potassium halides is strengthened further when we also consider the average hydrogen bond interaction energy between water molecules in the bulk in the same manner as our previous work.[52] This is calculated by first identifying bulk water molecules as described in the Materials and Methods section. Next, we determine which neighboring water molecules are donating hydrogen bonds to a central bulk water molecule. A neighboring water molecule is deemed to be donating a hydrogen bond to the central water molecule if it simultaneously satisfies two criteria: the neighboring water molecule oxygen is within a distance to the central water molecule oxygen corresponding to the first minimum in the O_w-O_w RDF (see Figure S3a), and at least one of the neighboring water molecule hydrogens is within a distance to the central water molecule oxygen corresponding to the first minimum in the O_w-H_w RDF (see Figure S3b). Once this condition is satisfied, the total enthalpic interaction between the two water molecules is calculated, as described in the Materials and Methods section. This process is repeated for every bulk water molecule in the simulation over 30 iterations to produce a distribution of bulk water−water hydrogen bond interaction energies. The resulting distributions can be seen in Figure S4a,b and are then fit using a Gaussian function to determine the average hydrogen bond interaction energy. These results are shown in Figure 2. Here, it can be seen that the average hydrogen bond interaction energy between two bulk water molecules is only negligibly altered in the presence of each of the four salt species, again indicating only short-range perturbations to water structure and enthalpic interactions as a result of the ions in solution.

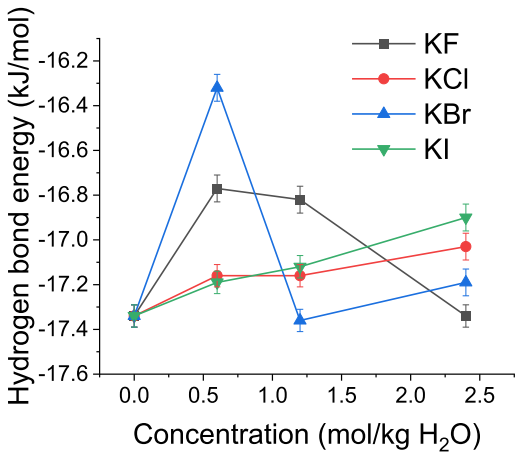

Figure 2. Average hydrogen bond interaction energy between bulk water molecules as a function of solute concentration. Average hydrogen bond interaction energy is calculated by first calculating the total interaction energy between individual pairs of bulk water molecules that are deemed to be hydrogen-bonded and fitting the resultant distribution with a Gaussian function. The displayed error bars correspond to the calculated error in the Gaussian peak location.

To investigate the range over which ions perturb water structure further, the average enthalpic interaction ΔH between a central potassium halide anion and surrounding water molecules as a function of distance can be considered. These results are shown in Figure 3. From this data, it is clear

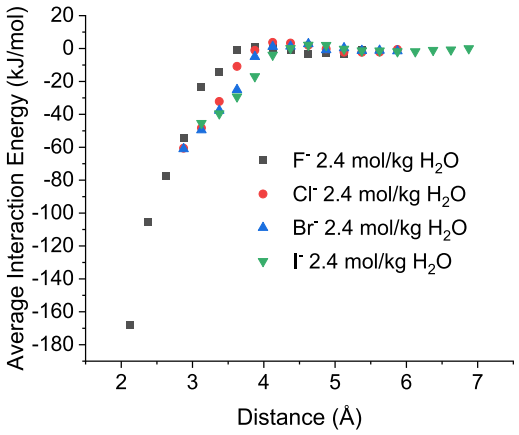

Figure 3. Average enthalpic interaction strength (ΔH) between a central potassium halide anion and its surrounding water molecules at a given distance. The enthalpic interaction strength between two molecules calculated as the sum of the Lennard-Jones and Coulomb potential calculated using the standard Lorentz−Berthelot mixing rules (see Table S1). Only data for the highest concentration of 2.4 mol/kg H_2O samples is shown for clarity (see Figure S5 for the remaining data sets).

that at small distances, below ∼3.5 Å, there are significant enthalpic interactions between the central anion and the surrounding water molecules, shown by negative values of average interaction energy. However, at larger distances, this quickly decays toward 0, indicating negligible enthalpic interactions between anions and water molecules in solution at distances above ∼4.0−4.5 Å.

To quantify the distance over which the anion has a favorable enthalpic interaction with the surrounding water molecules, a linear function was fit to the data shown in Figure 3 at low distances. The distance cutoff for the linear fits was varied for each salt to correspond to the region over which ΔH shows roughly linear behavior with distance. Details of the range over which the linear fits were performed, the resultant gradients and intercepts of the linear fits, and the quality of fit through the calculated R^2 value are shown in Tables S4a−d and S5a−d for each case. Points were chosen such that the range was consistent for each concentration of each salt; the quality of fit indicated by the R^2 value was suitably high (above 0.95), and the maximum number of possible points was used. The linear fits were then extrapolated to determine the distance at which $\Delta H = 0$, as demonstrated using example data in Figure S6. This procedure yields an apparent enthalpic interaction distance for each potassium halide anion at each of the three concentrations studied. The calculated distances for each concentration, in turn, were then extrapolated back to 0 concentration to yield a final value for the enthalpic interaction distance $r_{\Delta H=0}$ for each potassium halide anion, as shown in Figure S7. The resultant distances are shown in Table 2. These results show that with increasing ionic radius the distance over which the anion interacts enthalpically with water molecules

https://doi.org/10.1021/acs.jpcb.1c06728
J. Phys. Chem. B 2021, 125, 12774−12786

Table 2. Enthalpic Interaction Distances for Each Potassium Halide Anion Species Determined by Monitoring the Enthalpic Interaction Energy between the Potassium Halide Anion and the Surrounding Water Molecules as a Function of Distance[a]

potassium halide anion	enthalpic interaction distance (Å)	cutoff distance for first hydration shell (Å)
F^-	3.40 ± 0.02	3.21
Cl^-	4.03 ± 0.04	3.81
Br^-	4.21 ± 0.05	4.20
I^-	4.45 ± 0.03	4.49

[a]The final values reported are the enthalpic interaction distances extrapolated to 0 concentration for each potassium halide species. Cutoff distances for the first hydration shell for each potassium halide anion included. These are defined as the location of the first minimum in the X–O_w RDF, where X is the potassium halide anion species. The displayed uncertainties correspond to the calculated uncertainty in the y intercept of the linear fits shown in Figure S7.

$r_{\Delta H=0}$ is greater; however, the total enthalpic interaction, as shown by Table 1, is weaker. Table 2 also compares these results to the cutoff distances for the first hydration shell around each potassium halide anion, as described previously as corresponding to the location of the first minimum in the X–O_w RDF, where X is the potassium halide anion species. Here, we observe that for the smaller anion species F^- and Cl^- the enthalpic interaction distance $r_{\Delta H=0}$ extends outside the first hydration shell; however, for the largest anion species Br^- and I^-, $r_{\Delta H=0}$, the two quantities are approximately equal. These results indicate that $r_{\Delta H=0}$ varies more weakly with anionic species than the ability of the anion to form ordered hydration shells.

Water Dipole Orientation. The length over which potassium halides perturb water can also be considered by monitoring perturbations to water structure through the ion–water dipole angle θ, as shown in Figure 1. Monitoring the water dipole angle distribution around molecules of interest in aqueous solution, whether this be solutes or bulk water molecules, has been previously employed to investigate the structural perturbation in aqueous solution through neutron scattering and molecular dynamic simulation techniques.[19,32] In this work, we calculate the dipole angle for water molecules around the potassium cation and halide anions, as well as around bulk water molecules, as described in the Materials and Methods section. Here, the dipole angle for a water molecule within the first hydration shell (water molecules that lie within a distance corresponding to the first minima in the relevant RDF) around an ion/bulk water molecule is calculated for every appropriately placed water molecule over several iterations. The results are then binned in intervals of 2° for plotting and normalized to the total number of calculated dipole angles, such that the area under the resultant distributions is equal to unity. This allows each of the different salt types and concentrations to be compared directly. The normalized distribution of dipole angles around the halide anion and potassium ion is reported in Figure 4. The data is fitted using a function containing two summed Gaussian components, as shown in eq 4, where y_0 is the vertical offset, A_x is the area under Gaussian peak x, w_x is the width of the Gaussian peak x, and x_{cx} is the peak location for Gaussian peak

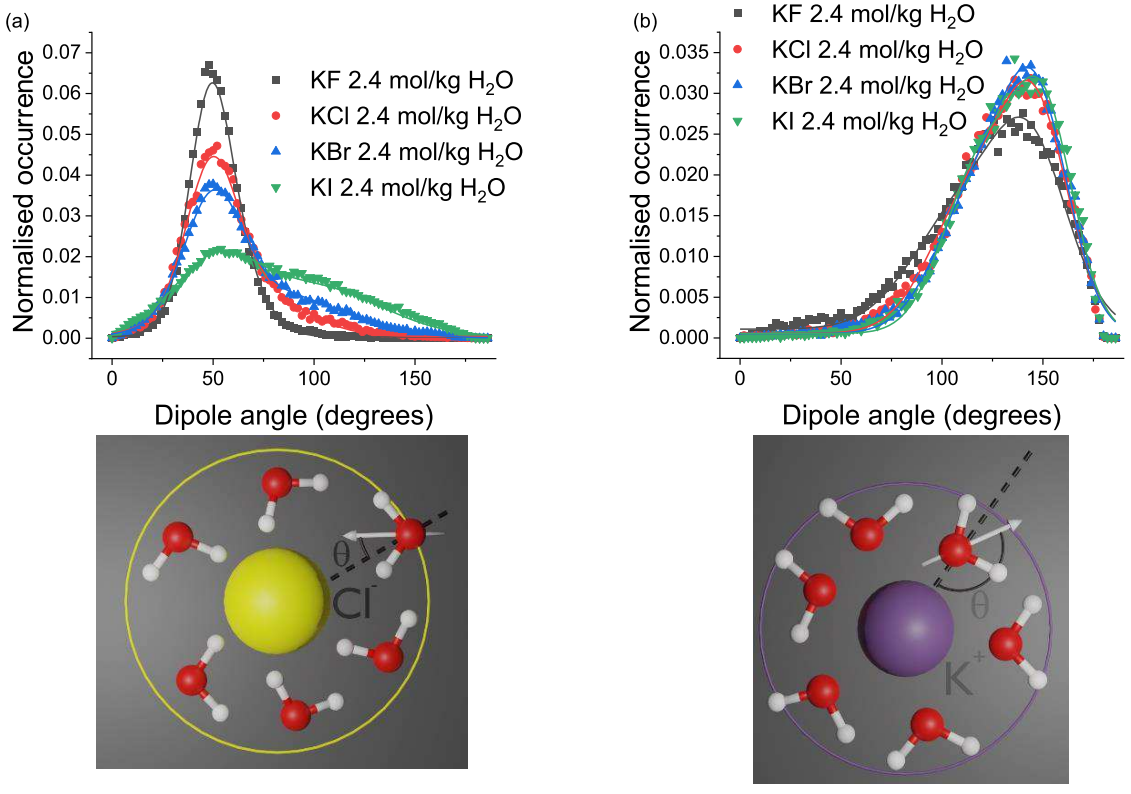

Figure 4. Distribution of dipole angles for water molecules hydrating a central halide anion (a) or potassium cation (b) within its first hydration shell. The dipole angle is defined as the angle between the vector pointing from the halide anion/potassium ion to the hydrating water oxygen and the vector corresponding to the hydrating water molecular dipole, as shown in Figure 1. Values normalized to the total number of data points. Only data for the highest concentration of 2.4 mol/kg H_2O samples is shown for clarity with the remaining data shown in Figure S8.

https://doi.org/10.1021/acs.jpcb.1c06728
J. Phys. Chem. B 2021, 125, 12774–12786

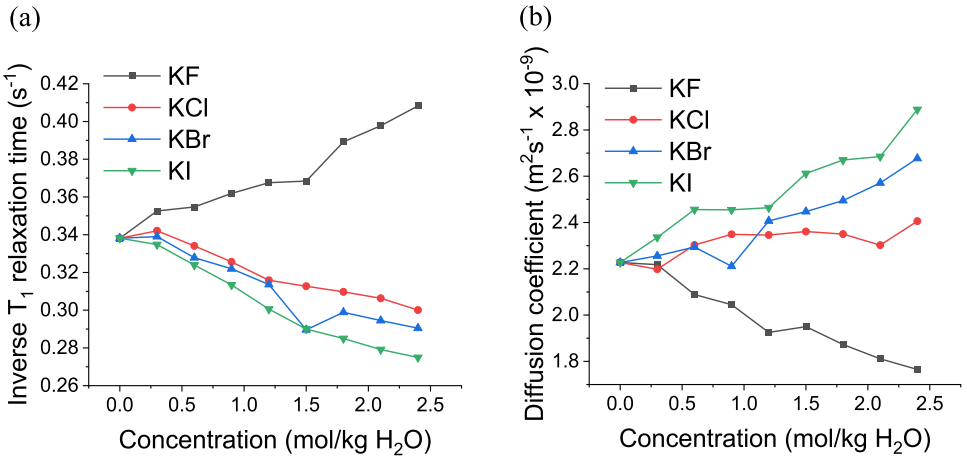

Figure 5. Inverse T_1 decay time (a) and diffusion coefficient D (b) from NMR experiments as a function of solute concentration.

x. The resultant fitting parameters for the water dipole angle distribution data around the halide anions and potassium cation at each of the three studied concentrations with associated uncertainties are reported in the Supporting Information (Tables S4a−d and S5a−d). We also report the calculated peak location, the full width at half-maximum (FWHM), and quality of fit through the calculated R^2 value for each case

$$y = y_0 + \frac{A_1}{w_1\sqrt{\frac{\pi}{2}}} \exp -2\left(\frac{x - x_{c1}}{w_1}\right)^2 + \frac{A_2}{w_2\sqrt{\frac{\pi}{2}}} \exp -2\left(\frac{x - x_{c2}}{w_2}\right)^2 \quad (4)$$

Figure 4a,b shows that all ions induce a local structure in the first hydration shell due to interactions between the charge on the halide anion/potassium cation and the partial charges located on the water molecule hydrogen/oxygen. This is shown by a peak in the normalized dipole angle distribution at ∼50° for water in the first hydration shell of halide anions and at ∼155° for water in the first hydration shell of potassium cations. For water in the first hydration shell of halide anions, the peak occurs at lower values than for water in the first hydration shell of potassium cations. This is because the surrounding water molecules will tend to point one positively charged hydrogen toward the negatively charged halide anion, as opposed to pointing both positively charged hydrogens away from the potassium cation, as illustrated in Figure 1.

As one moves down the halide group in the periodic table from F to I, the ionic radius increases from 119 to 206 pm[71] and therefore the absolute ionic charge density decreases from 0.142 to 0.027 e/Å^3. As seen in Figure 4a, with decreasing anionic charge density, we observe that the peak height in the anionic water dipole angle distribution reduces and the peak width broadens. We also observe the emergence of a second Gaussian component at higher angles, occurring at ∼90° in the most extreme case of KI, therefore suggesting an increasingly disordered hydration shell with increasing ionic radius of the halide anion.

Next, we consider the water dipole angle distribution around the potassium cation (Figure 4b). Here, we observe that as the ionic radius of the associated potassium halide anion increases, the water dipole angle distribution around the potassium cation is unchanged, showing a single clear peak at ∼155° in the case of KCl, KBr, and KI at 2.4 mol/kg H_2O. However, in the case of KF at 2.4 mol/kg H_2O, the peak moves inwards to ∼145° while becoming shorter and broader. This dependence of the water dipole angle distribution around the potassium cation on the species of the corresponding halide anion suggests nonlocal longer-ranged effects on water structure induced by the halide anion. However, if we consider the water dipole angle distribution around the potassium cation at the lower concentrations of 0.6 and 1.2 mol/kg H_2O (see Figure S8), we observe that the water dipole angle distribution is unchanged for all four salt species, suggesting local short-ranged effects of the halide anions on water structure. The dependence of the water dipole angle distribution around the potassium cation on the species of the corresponding halide anion at high concentration can also be explained by local short-ranged effects. At the highest concentration of 2.4 mol/kg H_2O, the average distance between ions is calculated to be 4.2−4.4 Å, and the anion-K^+ coordination number begins to approach unity (see Table S3). As shown in Table 2, the first hydration shell of water around any of the ion species discussed in this work extends from 3.21 Å in the case of F^- to 4.49 Å in the case of I^-. Therefore, at a potassium halide concentration of 2.4 mol/kg H_2O, it is highly likely that a significant proportion of water molecules are in the first hydration shell of two or more separate ions and are therefore experiencing strong enthalpic interactions from multiple sources, which in turn will perturb the water dipole angle distribution. The influence of the halide anion species on the water dipole angle distribution around a potassium ion is therefore due to a local effect of overlapping/directly interacting hydration shells around the ions, rather than long-ranged effects induced by the anions, as these would be evident at the lower concentrations. The evidence for short-ranged rather than long-ranged effects on water structure by the potassium halide ions studied here is strengthened further as the dipole angle distribution around central bulk water molecules is unchanged for all salt species at all studied concentrations (see Figure S9). However, we must also mention here that earlier neutron scattering work by Soper and Weckström found subtle perturbations to the ion−water dipole angle distribution in the second ion hydration shell, but that these perturbations are far weaker than those found in the first hydration shell.[32]

https://doi.org/10.1021/acs.jpcb.1c06728
J. Phys. Chem. B 2021, 125, 12774−12786

NMR Dynamics of Potassium Halide Solutions. NMR experiments were completed on KF, KCl, KBr, and KI over a range of 0−2.4 mol/kg H_2O in 0.3 mol/kg H_2O increments to observe dynamic perturbations to water in the presence of the ions. To determine their impact on water dynamics, here we report the inverse T_1 decay time, proportional to the rotational correlation time of the water molecules (Figure 5a), and the diffusion coefficient (Figure 5b). The raw NMR data used to calculate these values is presented in Figures S11 and S12. In both instances, the calculated inverse T_1 and D measurements represent an ensemble average of the motions of individual water molecules. This is because the time period of one Larmor precession (approximately 23 ns at 43 MHz and 2.5 ns at 400 MHz) far exceeds the rotational correlation time of the water molecules (on the order of picosecond). Therefore, while the different microenvironments present in the solutions will be influencing the measured T_1 and D values separately, they will fast average to a single value.

These results are in good agreement with NMR results on aqueous potassium halides reported by Laage et al.[72] Using the inverse T_1 decay time data for each salt species, it is possible to quantify the perturbation to the rotational correlation time of the water molecules in the hydration shell of the various ionic species. This method is identical to that outlined by Engel and Hertz in 1968.[36] The method assumes that within an aqueous solution containing two separate ionic species, such as the potassium halide salts discussed in this work, there exist three distinct rotational correlation times for water molecules. Each of these rotational correlation times is attributed to water molecules in each of the three different microenvironments present in the solution: water molecules located in the potassium cation hydration shell τ_c^+, water molecules located in the halide anion hydration shell τ_c^-, and the remaining bulk water molecules not located in the hydration shell of either the potassium cation or the halide anion τ_c^0. The results for the previous sections (Table 1 and Figures 2 and 3) all suggest that potassium halide ions only significantly perturb water structure and energetics within their first hydration shells. This is therefore in good agreement with the assumption required by the method of Engel and Hertz.[36]

As mentioned previously, the inverse T_1 relaxation time is proportional to the rotational correlation time of the water molecules. The measured inverse T_1 relaxation time for a particular aqueous solution is therefore proportional to the weighted average of the three rotational correlation times for each of the three environments described above. This is described mathematically in eq 5, where one mole of salt dissolves into $\nu^{\pm}$ moles of cations/anions, both equal to unity in the simple case of potassium halides, $n_h^{\pm}$ is the coordination number for the cation/anion, and c is the concentration of the salt in mol/kg H_2O. A factor of 55.5 originates from the molarity of pure water.[36] The coefficient for each of the three rotational correlation times described in eq 5 is therefore equivalent to the fraction of water molecules located in each of the three environments

$$\frac{1}{T_1} \propto \left[1 - \frac{\nu^+ n_h^+ c}{55.5} - \frac{\nu^- n_h^- c}{55.5}\right]\tau_c^0 + \frac{\nu^+ n_h^+ c}{55.5}\tau_c^+ + \frac{\nu^+ n_h^+ c}{55.5}\tau_c^- \tag{5}$$

We now also consider a form of the Jones−Dole equation,[73] which describes the ratio between the viscosity of a solution to the viscosity of pure water as a polynomial function of concentration. A version of this equation as applicable to T_1 relaxation measurements is shown in eq 6, where $T_{1,0}$ is the relaxation time of pure water and c is the solute concentration in mol/kg H_2O

$$\frac{\frac{1}{T_1}}{\frac{1}{T_{1,0}}} = 1 + Bc + Cc^2 + \cdots \tag{6}$$

We now allow the B coefficient to be expressed as the sum of the contributions from the rotational correlation times of water molecules in the potassium cation hydration shell B^+ and the rotational correlation times of water molecules in the halide anion hydration shell B^-, as shown in eq 7

$$B = B^+ + B^- \tag{7}$$

We then assume that for low concentrations where $\frac{1}{T_1}$ is linearly dependent on concentration, such is the case for the potassium halides studied here, as shown by Figure 5a, that only the first two terms of the polynomial expression shown in eq 6 are necessary to sufficiently describe the solution. This in turn means we can also safely assume that the rotational correlation times of water molecules in the hydration shells of the potassium cation or the halide anion are independent of concentration in this concentration range. We can then combine eqs 5−7 to form eq 8, which describes the rotational correlation times for water molecules in the hydration shell of the potassium cation/halide anion normalized to the rotational correlation time of pure water

$$\frac{\tau_c^{\pm}}{\tau_c^0} = 1 + \frac{55.5}{n^{\pm}}B^{\pm} \tag{8}$$

Finally, to use this expression, we must already have knowledge of the B parameter for one of the ion species present in any of the potassium halide salts studied here. The simplest way of achieving this is to state that two ion species have identical B parameters. For this, we again follow the procedure of Engel and Hertz[36] who state that $B(Cl^-) = B(K^+)$. While this is a simple assumption, we can consider several parameters relating to the two ion species to justify that this is the most reasonable assumption as the potassium cation and chloride anion are the most similar ions. These comparisons are shown in Table 3.

Table 3. Comparison of Ionic Radius, Enthalpy of Hydration, Coordination Number, and Enthalpy of Hydration per Coordinated Water Molecule to Determine Which Halide Anion Is Most Similar to the Potassium Cation[a]

ion species	ionic radius[71] (pm)	ΔH_{EPSR} (kJ/mol)	coordination number	ΔH_{EPSR} per coordinated water (kJ/mol)
K^+	152	−360 ± 2	6.4	−56.3 ± 0.3
F^-	119	−550 ± 50	6.3	−87 ± 8
Cl^-	167	−290 ± 10	7.0	−41 ± 1
Br^-	182	−241 ± 5	8.7	−27.7 ± 0.6
I^-	206	−250 ± 30	10.1	−25 ± 3

[a]This demonstrates that the ionic radii ΔH_{EPSR} and ΔH_{EPSR} per coordinated water are the most similar between K^+ and Cl^- ions. Coordination number is most similar between K^+ and F^- ions. Therefore, overall, K^+ and Cl^- are the most similar.

https://doi.org/10.1021/acs.jpcb.1c06728
J. Phys. Chem. B 2021, 125, 12774−12786

We can now fit the data shown in Figure 5a using eq 6 using the assumption that terms beyond Bc are negligible to extract the B parameter for each potassium halide ion. This can then be combined with the coordination numbers, calculated according to the cutoff distances shown in Table 2 and given in Table 3, and assuming that $B(Cl^-) = B(K^+)$ to yield the B parameter for each ion and the rotational correlation time for water molecules in the hydration shell of the potassium cation/halide anion normalized to the rotational correlation time of pure water, as shown in Table 4. These results show that the rotational dynamics of water are retarded in the hydration shell of F^- but accelerated in the hydration shells of Cl^-, K^+, Br^-, and I^- (listed in order of decreasing normalized rotational correlation time and therefore increasing acceleration).

Table 4. Calculated Parameters for Each of the Five Ion Species Discussed in This Work[a]

ion species	B (kg H_2O/mol)	n_h	$\frac{\tau_c^{\pm}}{\tau_c^0}$
K^+	−0.0264	6.4	0.77
F^-	0.1072	6.3	1.94
Cl^-	−0.0264	7	0.79
Br^-	−0.0387	8.7	0.75
I^-	−0.0592	10.1	0.67

[a]NMR B parameter calculated through linear fits to the inverse T_1 relaxation data given in Figure 5a according to eq 6, coordination number n_h calculated through EPSR using cutoff distances described in Table 2, and calculated rotational correlation time for water molecules in the hydration shell of the ion normalized to the rotational correlation time for pure water $\frac{\tau_c^{\pm}}{\tau_c^0}$ according to eq 8.

We can now apply the same technique to the diffusion coefficient data, using the same assumptions as applied to the inverse T_1 relaxation data (see eqs S2−S4 for full details) and using the relation that the inverse T_1 relaxation time is proportional to the inverse water molecule diffusion coefficient[36] $\frac{1}{T_1} \propto \frac{1}{D}$ (see Figure S10) to determine the diffusion coefficient for water molecules in the hydration shells of the potassium halide ions $D^{\pm}$ normalized to the inverse diffusion coefficient for pure water D^0, as shown in Table 5. Just as for the normalized rotational correlation time results, shown in Table 4, these results show that the diffusive dynamics of water are retarded in the hydration shell of F^- and accelerated in the hydration shell of Cl^-, K^+, Br^-, and I^- (listed in order of increasing acceleration). These results demonstrate that with increasing ion size, and hence decreasing charge density, that both the rotational and diffusive dynamics of water molecules in the ion's first hydration shell are accelerated.

Table 5. Calculated Parameters for Each of the Five Ion Species Discussed in This Work[a]

ion species	B (kg H_2O/mol)	n_h	$\frac{D^{\pm}}{D^0}$
K^+	0.0422	6.4	1.13
F^-	0.0645	6.3	0.47
Cl^-	0.0422	7	1.12
Br^-	−0.0139	8.7	1.59
I^-	−0.1319	10.1	1.62

[a]NMR B parameter calculated through linear fits to the normalized inverse diffusion coefficient D data given in Figure 5b according to eq S3, coordination number n_h calculated through EPSR using cutoff distances described in Table 2, and calculated diffusion coefficient for water molecules in the hydration shell of the ion normalized to the diffusion coefficient for pure water $\frac{D^{\pm}}{D^0}$ according to eq S4.

DISCUSSION

Our results are in agreement with the growing consensus[1,2,22,25,30−42] that simple monovalent ions, such as the potassium halide ions discussed in this work, only perturb the structure of water within their first hydration shells. We first consider the enthalpy of hydration, defined as the heat released when a mole of the ion dissolves in a large amount of water forming an infinite dilute solution in the process.[69] This term would contain three contributions: the ion−ion interactions, the ion−water interactions, and the water−water interactions. The requirement of an infinitely dilute solution means that the ion−ion interactions are negligible by definition. Our data shown in Table 1 shows that the enthalpy of hydration, calculated by only considering structural data on water molecules in the first hydration shell of an ion, is in close agreement with the experimental enthalpy of hydration.[70,74] This demonstrates that by only considering short-ranged interactions in aqueous solutions of potassium halides, we can recapture bulk experimental properties. Figure 2 then shows that the average hydrogen bond interaction energy between two bulk water molecules is essentially unaffected by the potassium halide salts KF, KCl, KBr, and KI up to a maximum studied concentration of 2.4 mol/kg H_2O. These two observations, combined with the requirement of an infinitely dilute solution, show that of the three contributions to the enthalpy of hydration listed previously, the ion−ion interactions, the ion−water interactions, and the water−water interactions, only the short-ranged ion−water interactions are significant and the other two contributions are negligible. This is further supported by Figure 3, which demonstrates that anions only have a significant enthalpic interaction, shown by negative enthalpic interaction energies, with water molecules at distances below ∼4.5 Å. We also use this data to quantify the range over which each potassium halide anion has significant enthalpic interactions with the neighboring water molecules. These results show that the enthalpic interactions between halide anions and neighboring water molecules decay to $\Delta H = 0$ at distances that closely correspond with the cutoff distance of the first hydration shell (see Table 2).

The water dipole angle distribution around halide anions shows a strong dependence on ion species, as shown by Figure 4a for the water dipole angle distribution around the halide anions at a concentration of 2.4 mol/kg H_2O. At the two lower concentrations of 0.6 and 1.2 mol/kg H_2O, the water dipole angle distribution around the potassium cation is unchanged with halide anion species; however, at the highest concentration of 2.4 mol/kg H_2O, where the overlap of ion hydration shells becomes significant, the dipole angle distribution around the potassium cation varies with halide anion species, as shown by Figure 4b. This is therefore likely a local effect due to the direct interaction between hydration shells of neighboring ions. We also observe that the dipole angle distribution around bulk water molecules is unchanged at all concentrations for all salt species (see Figure S9), suggesting local rather than global effects.

We also observe correlations between the dipole angle distribution (Figure 4a,b) and several key parameters that

https://doi.org/10.1021/acs.jpcb.1c06728
J. Phys. Chem. B 2021, 125, 12774−12786

describe the system. Previous simulation and infrared spectroscopy studies have shown that the rotational dynamics of water in the hydration shell of potassium halide ions observe a trend from slow to fast with F^-, Cl^-, Br^-, K^+, I^-.[41,75] This order correlates with the height of the peak in the water dipole angle distribution around the ion, as these also occur in the same order. If we consider the normalized rotational correlation time data (Table 4) for water molecules in the hydration shell of potassium halide ions and the normalized diffusion coefficient data (Table 5), we observe the order from slow to fast as F^-, Cl^-, K^+, Br^-, I^-. Considering these results together, we can observe that within the halide anion series (F^-, Cl^-, Br^-, I^-), that water molecules are increasingly mobile, in both their rotational and diffusive motions, with increasing halide anion size when monitored using multiple techniques. However, it becomes difficult to confidently state where the dynamics of water molecules in the hydration shell of the potassium cation fall on these scales. This difficultly likely arises from the assumptions involved with different experimental techniques. Within the simulation and EPSR studies, water molecules and ions are described with a relatively simple potential, consisting of a Lennard-Jones and Coulomb component.[32,75] Within our NMR approach, introduced by Engel and Hertz,[36] we make the assumption that the NMR B parameter derived from both inverse T_1 and inverse diffusion coefficient D data is identical for K^+ and Cl^-, as described previously. This is almost certainly not the case but is still a useful way of observing the relative perturbing ability of ions on the rotational and diffusive dynamics of water molecules within their hydration shells. We must also consider the difference in the nature of cationic vs anionic hydration. In positively charged cations, water molecules within the first hydration shell will tend to orient both hydrogens away from the central cation, whereas, in negatively charged anions, water molecules within the first hydration shell will tend to orient one hydrogen toward the central anion. This will certainly result in subtle differences in the mechanism for hydrogen bond switching events resulting in diffusive and rotational motion of the water molecules within ionic hydration shells, as explored by Laage et al.[72]

We can now consider the relation between structural perturbation and dynamic perturbation within the first hydration shell of halide anions. If we consider the water dipole angle distribution (Figure 4a) alongside the halide anion−O_w RDFs (Figure S1), we observe that both the peak of the water dipole angle distribution around the halide anion and the first peak of the anion−O_w RDF become shorter and broader with increasing size of the halide anion. Simply put, it can therefore be said that water molecules are less structurally constrained in the hydration shells around the halide anions with increasing anion sizes and are freer to adopt a larger range of distances and orientations. As stated above, we also observe that with increasing halide anion size, water molecules in the first hydration shell exhibit accelerated rotational and diffusive dynamics. It would therefore appear that how structurally constrained the water is within the hydration shell of an ion plays a key role in the dynamics of the water molecules. Less constraint over the preferred orientation and distance of the hydrating water molecules relative to the central halide anion likely means that they can more often be found in an appropriate conformation to undergo hydrogen bond switching, and a reduced enthalpic interaction provides a lower-energy barrier to carry out the hydrogen bond switching event, resulting in the increased dynamics.

This reduction of how structurally constrained water molecules are in the first hydration shell around halide anions is also reflected in bulk thermodynamic properties, namely, the calculated entropy of hydration at the experimental temperature $T\Delta S_{solv}$ shown in Table 1. We observe that with a less structurally constrained hydration shell with increasing halide anion size, shown by the shorter and broader peaks in the water dipole angle distribution (Figure 4a) and the anion−O_w RDFs (Figure S1), there is a reduction in the entropy penalty associated with including the halide anion into the water network at constant temperature $T\Delta S_{solv}$ shown by less negative values of $T\Delta S_{solv}$ with increasing halide anion size (Table 1). This is unsurprising, as less structurally constrained water molecules are clearly free to explore a larger variety of different states, resulting in a reduced entropic penalty by definition. We also observe increased rotational (Table 4) and diffusive (Table 5) dynamics of water molecules, shown by the calculated $\frac{\tau_c^{\pm}}{\tau_c^0}$ and $\frac{D^{\pm}}{D^0}$ values for each ion in the first hydration shells of the halide anions with increasing anion size. These increased rotational and diffusive water molecule dynamics suggest that not only are water molecules free to explore a larger variety of different conformations but they can do so at a faster rate. This is therefore also consistent with the observed reduced entropic penalty of hydration shown by less negative values of $T\Delta S_{solv}$ with increasing anion size.

CONCLUSIONS

The conclusions drawn here, that the effects of ions are local rather than global, clearly hold for simple monovalent electrolytes such as potassium halides. We observe that with increasing ion size, and therefore decreasing ion charge density, water molecules in the first hydration shell are less well structured. This is coupled with a less negative enthalpy of hydration, as electrostatic interactions between the ions and surrounding water molecules become less favorable as the hydration shell becomes more disordered. The rotational and diffusive dynamics of water molecules in the first hydration shell of the ions are also observed to be accelerated with increasing ion size. The combined effects of a more structurally disordered hydration shell and increased water molecule dynamics result in a less negative entropy of hydration. These observations suggest that we can study these short-ranged local environments to calculate bulk properties of the complete aqueous system, such as the enthalpy of hydration ΔH_{solv}, and reveal correlations between other bulk properties, such as the entropy of hydration ΔS_{solv}. However, we have previously observed more global effects with divalent and polyatomic ions such as Mg^{2+} and $(ClO_4)_2$, as well as osmolytes such as trimethylamine N-oxide,[52] that not only perturb water in the first hydration shells of the solutes but go on to significantly perturb hydrogen bonding and water structure in the bulk. Recent molecular dynamics studies by Gaiduk et al.[19] also suggest that while water in the hydration shells of simple salts such as NaCl may appear to only be perturbed in the immediate vicinity of the ions, water molecules can experience polarizability changes at much larger distances. These more complicated solutes merit further investigation through complimentary techniques such as those illustrated in this work to determine at which point solutes begin to perturb aqueous solution more globally.

https://doi.org/10.1021/acs.jpcb.1c06728
J. Phys. Chem. B 2021, 125, 12774−12786

■ ASSOCIATED CONTENT

Supporting Information

The Supporting Information is available free of charge at https://pubs.acs.org/doi/10.1021/acs.jpcb.1c06728.

Important parameters/EPSR results used to inform analysis routines and calculate final values reported in this work; Lennard-Jones parameters and charges on each atom species, relevant RDFs and locations of relevant minima in RDFs, interaction energy distributions, coordination numbers, remaining data sets for 0.6 and 1.2 mol/kg H_2O concentrations not shown in the main paper, derivations of equations used to deconvolute diffusion coefficient data, and justification of $\frac{1}{T_1} \propto \frac{1}{D}$ (PDF)

■ AUTHOR INFORMATION

Corresponding Author

Lorna Dougan − *School of Physics and Astronomy, University of Leeds, Leeds LS2 9JT, U.K.; Astbury Centre for Structural and Molecular Biology, University of Leeds, Leeds LS2 9JT, U.K.;* orcid.org/0000-0002-2620-5827; Email: L.Dougan@leeds.ac.uk

Authors

Harrison Laurent − *School of Physics and Astronomy, University of Leeds, Leeds LS2 9JT, U.K.*

Daniel L. Baker − *School of Physics and Astronomy, University of Leeds, Leeds LS2 9JT, U.K.;* orcid.org/0000-0002-5145-3320

Alan K. Soper − *ISIS Facility, STFC Rutherford Appleton Laboratory, Didcot OX11 0QX, U.K.*

Michael E. Ries − *School of Physics and Astronomy, University of Leeds, Leeds LS2 9JT, U.K.;* orcid.org/0000-0002-8050-3200

Complete contact information is available at: https://pubs.acs.org/10.1021/acs.jpcb.1c06728

Notes

The authors declare no competing financial interest.

The data associated with the study can be found here: https://doi.org/10.5518/1061.

■ ACKNOWLEDGMENTS

The project was supported by a grant from the Engineering and Physical Sciences Research Council (EPSRC) (EP/P02288X/1) to L.D. H.L. is supported by an ISIS Facility Development and Utilisation Studentship and an EPSRC DTA studentship. The authors acknowledge ISIS Neutron and Muon Source on which the neutron diffraction experiments were completed on the SANDALS instrument. The authors thank all members of the Dougan group for helpful discussion and feedback.

■ REFERENCES

(1) Bakker, H. J. Structural Dynamics of Aqueous Salt Solutions. *Chem. Rev.* **2008**, *108*, 1456−1473.

(2) Ohtaki, H.; Radnai, T. Structure and Dynamics of Hydrated Ions. *Chem. Rev.* **1993**, *93*, 1157−1204.

(3) Marcus, Y. Effect of Ions on the Structure of Water: Structure Making and Breaking. *Chem. Rev.* **2009**, 1346−1370.

(4) van der Vegt, N. F. A.; Haldrup, K.; Roke, S.; Zheng, J.; Lund, M.; Bakker, H. J. Water-Mediated Ion Pairing: Occurrence and Relevance. *Chem. Rev.* **2016**, *116*, 7626−7641.

(5) Brini, E.; Fennell, C. J.; Fernandez-Serra, M.; Hribar-Lee, B.; Lukšič, M.; Dill, K. A. How Water's Properties Are Encoded in Its Molecular Structure and Energies. *Chem. Rev.* **2017**, *117*, 12385−12414.

(6) Laurent, H.; Soper, A.; Dougan, L. Biomolecular Self-Assembly under Extreme Martian Mimetic Conditions. *Mol. Phys.* **2019**, *117*, 3398−3407.

(7) Chen, X.; Yang, T.; Kataoka, S.; Cremer, P. S. Specific Ion Effects on Interfacial Water Structure near Macromolecules. *J. Am. Chem. Soc* **2007**, *129*, 12272−12279.

(8) Maity, H.; Muttathukattil, A. N.; Reddy, G. Salt Effects on Protein Folding Thermodynamics. *J. Phys. Chem. Lett.* **2018**, *9*, 5063−5070.

(9) Murakami, S.; Hayashi, T.; Kinoshita, M. Effects of Salt or Cosolvent Addition on Solubility of a Hydrophobic Solute in Water: Relevance to Those on Thermal Stability of a Protein. *J. Chem. Phys.* **2017**, *146*, No. 055102.

(10) Kammerer, J.; Carle, R.; Kammerer, D. R. Adsorption and Ion Exchange: Basic Principles and Their Application in Food Processing. *J. Agric. Food Chem.* **2011**, *59*, 22−42.

(11) Yaseen, D. A.; Scholz, M. *Textile Dye Wastewater Characteristics and Constituents of Synthetic Effluents: A Critical Review*; Springer: Berlin, 2019; Vol. *16*.

(12) Mamelkina, M. A.; Cotillas, S.; Lacasa, E.; Sáez, C.; Tuunila, R.; Sillanpää, M.; Häkkinen, A.; Rodrigo, M. A. Removal of Sulfate from Mining Waters by Electrocoagulation. *Sep. Purif. Technol.* **2017**, *182*, 87−93.

(13) Castro, J.; Asta, M. P.; Galve, J. P.; Azañón, J. M. Formation of Clay-Rich Layers at the Slip Surface of Slope Instabilities: The Role of Groundwater. *Water* **2020**, *12*, No. 2639.

(14) Daly, L.; Lee, M. R.; Piazolo, S.; Griffin, S.; Bazargan, M.; Campanale, F.; Chung, P.; Cohen, B. E.; Pickersgill, A. E.; Hallis, L. J.; Trimby, P. W.; Baumgartner, R.; Forman, L. V.; Benedix, G. K. Boom Boom Pow: Shock-Facilitated Aqueous Alteration and Evidence for Two Shock Events in the Martian Nakhlite Meteorites. *Sci. Adv.* **2019**, *5*, No. eaaw5549.

(15) Orosei, R.; Lauro, S. E.; Pettinelli, E.; Cicchetti, A.; Coradini, M.; Cosciotti, B.; Di Paolo, F.; Flamini, E.; Mattei, E.; Pajola, M.; Soldovieri, F.; Cartacci, M.; Cassenti, F.; Frigeri, A.; Giuppi, S.; Martufi, R.; Masdea, A.; Mitri, G.; Nenna, C.; Noschese, R.; Restano, M.; Seu, R. Radar Evidence of Subglacial Liquid Water on Mars. *Science* **2018**, *361*, 490−493.

(16) Taubner, R. S.; Leitner, J. J.; Firneis, M. G.; Hitzenberger, R. Modelling the Interior Structure of Enceladus Based on the 2014's Cassini Gravity Data. *Origins Life Evol. Biospheres* **2016**, *46*, 283−288.

(17) Hussman, H. *Treatise on Geophysics*, 1st ed.; Spohn, T., Ed.; Elsevier: London, 2007; Vol. *10*.

(18) Baul, U.; Vemparala, S. Ion Hydration and Associated Defects in Hydrogen Bond Network of Water: Observation of Reorientationally Slow Water Molecules beyond First Hydration Shell in Aqueous Solutions of MgCl2. *Phys. Rev. E: Stat., Nonlinear, Soft Matter Phys.* **2015**, *91*, No. 012114.

(19) Gaiduk, A. P.; Galli, G. Local and Global Effects of Dissolved Sodium Chloride on the Structure of Water. *J. Phys. Chem. Lett.* **2017**, *8*, 1496−1502.

(20) Hpone Myint, K.; Ding, W.; Willard, A. P. The Influence of Spectator Cations on Solvent Reorganization Energy Is a Short-Range Effect. *J. Phys. Chem. B* **2021**, 1429.

(21) Zhao, L.; Ma, K.; Yang, Z. Changes of Water Hydrogen Bond Network with Different Externalities. *Int. J. Mol. Sci.* **2015**, *16*, 8454−8489.

(22) Collins, K. D.; Neilson, G. W.; Enderby, J. E. Ions in Water: Characterizing the Forces That Control Chemical Processes and Biological Structure. *Biophys. Chem.* **2007**, *128*, 95−104.

(23) Bruce, E. E.; Okur, H. I.; Stegmaier, S.; Drexler, C. I.; Rogers, B. A.; Van Der Vegt, N. F. A.; Roke, S.; Cremer, P. S. Molecular

Mechanism for the Interactions of Hofmeister Cations with Macromolecules in Aqueous Solution. *J. Am. Chem. Soc.* **2020**, *142*, 19094−19100.
(24) Nucci, N. V.; Vanderkooi, J. M. Effects of Salts of the Hofmeister Series on the Hydrogen Bond Network of Water. *J. Mol. Liq.* **2008**, *143*, 160−170.
(25) Okur, H. I.; Hladílková, J.; Rembert, K. B.; Cho, Y.; Heyda, J.; Dzubiella, J.; Cremer, P. S.; Jungwirth, P. Beyond the Hofmeister Series: Ion-Specific Effects on Proteins and Their Biological Functions. *J. Phys. Chem. B* **2017**, 1997−2014.
(26) Hofmeister, F. Zur Lehre Yon Der Wirkung Der Salze. *Arch. Exp. Pathol. Pharmakol.* **1888**, *24*, 247−260.
(27) Ball, P.; Hallsworth, J. E. Water Structure and Chaotropicity: Their Uses, Abuses and Biological Implications. *Phys. Chem. Chem. Phys.* **2015**, *17*, 8297−8305.
(28) Collins, K. D.; Washabaugh, M. W. The Hofmeister Effect and the Behaviour of Water at Interfaces. *Q. Rev. Biophys.* **1985**, *18*, 323−422.
(29) Hribar, B.; Southall, N. T.; Vlachy, V.; Dill, K. A. How Ions Affect the Structure of Water. *J. Am. Chem. Soc.* **2002**, *124*, 12302−12311.
(30) Lenton, S.; Rhys, N. H.; Towey, J. J.; Soper, A. K.; Dougan, L. Highly Compressed Water Structure Observed in a Perchlorate Aqueous Solution. *Nat. Commun.* **2017**, *8*, No. 919.
(31) Mancinelli, R.; Botti, A.; Bruni, F.; Ricci, M. A.; Soper, A. K. Hydration of Sodium, Potassium, and Chloride Ions in Solution and the Concept of Structure Maker/Breaker. *J. Phys. Chem. B* **2007**, *111*, 13570−13577.
(32) Soper, A. K.; Weckström, K. Ion Solvation and Water Structure in Potassium Halide Aqueous Solutions. *Biophys. Chem.* **2006**, *124*, 180−191.
(33) Mancinelli, R.; Botti, A.; Bruni, F.; Ricci, M. A.; Soper, A. K. Perturbation of Water Structure Due to Monovalent Ions in Solution. *Phys. Chem. Chem. Phys.* **2007**, *9*, 2959−2967.
(34) Ansell, S.; Barnes, A. C.; Mason, P. E.; Neilson, G. W.; Ramos, S. X-Ray and Neutron Scattering Studies of the Hydration Structure of Alkali Ions in Concentrated Aqueous Solutions. *Biophys. Chem.* **2006**, *124*, 171−179.
(35) Jeyachandran, Y. L.; Meyer, F.; Nagarajan, S.; Benkert, A.; Bär, M.; Blum, M.; Yang, W.; Reinert, F.; Heske, C.; Weinhardt, L.; Zharnikov, M. Ion-Solvation-Induced Molecular Reorganization in Liquid Water Probed by Resonant Inelastic Soft X-Ray Scattering. *J. Phys. Chem. Lett.* **2014**, *5*, 4143−4148.
(36) Engel, G.; Hertz, H. On the Negative Hydration. A Nuclear Magnetic Relaxation Study. *Ber. Bunsen-Ges. Phys. Chem.* **1968**, *72*, 808−834.
(37) Gulich, R.; Köhler, M.; Lunkenheimer, P.; Loidl, A. Dielectric Spectroscopy on Aqueous Electrolytic Solutions. *Radiat. Environ. Biophys.* **2009**, *48*, 107−114.
(38) Kondoh, M.; Ohshima, Y.; Tsubouchi, M. Ion Effects on the Structure of Water Studied by Terahertz Time-Domain Spectroscopy. *Chem. Phys. Lett.* **2014**, *591*, 317−322.
(39) Max, J.-J.; Gessinger, V.; Van Driessche, C.; Larouche, P.; Chapados, C. Infrared Spectroscopy of Aqueous Ionic Salt Solutions at Low Concentrations. *J. Chem. Phys.* **2007**, *126*, No. 184507.
(40) Giammanco, C. H.; Wong, D. B.; Fayer, M. D. Water Dynamics in Divalent and Monovalent Concentrated Salt Solutions. *J. Phys. Chem. B* **2012**, *116*, 13781−13792.
(41) Chowdhuri, S.; Chandra, A. Dynamics of Halide Ion-Water Hydrogen Bonds in Aqueous Solutions: Dependence on Ion Size and Temperature. *J. Phys. Chem. B* **2006**, *110*, 9674−9680.
(42) Schwierz, N.; Horinek, D.; Sivan, U.; Netz, R. R. Reversed Hofmeister Series—The Rule Rather than the Exception. *Curr. Opin. Colloid Interface Sci.* **2016**, *23*, 10−18.
(43) Rozov, A.; Khusainov, I.; El Omari, K.; Duman, R.; Mykhaylyk, V.; Yusupov, M.; Westhof, E.; Wagner, A.; Yusupova, G. Importance of Potassium Ions for Ribosome Structure and Function Revealed by Long-Wavelength X-ray Diffraction. *Nat. Commun.* **2019**, *10*, No. 2519.
(44) Black, C. B.; Huang, H. W.; Cowan, J. A. Biological Coordination Chemistry of Magnesium, Sodium, and Potassium Ions. Protein and Nucleotide Binding Sites. *Coord. Chem. Rev.* **1994**, *135−136*, 165−202.
(45) Langlois, V. Laboratory Evaluation at Different Ages. *Comprehensive Pediatric Nephrology*; Elsevier, 2008; pp 39−54.
(46) Pinho, S. P.; Macedo, E. A. Solubility of NaCl, NaBr, and KCl in Water, Methanol, Ethanol, and Their Mixed Solvents. *J. Chem. Eng. Data* **2005**, *50*, 29−32.
(47) Soper, A. K. *Rutherford Appleton Laboratory Technical Report*, RAL-TR-2011-013; Rutherford Appleton Laboratory, 2011; Vol. *RAL-TR-201*.
(48) Soper, A. K. Tests of the Empirical Potential Structure Refinement Method and a New Method of Application to Neutron Diffraction Data on Water. *Mol. Phys.* **2001**, *99*, 1503−1516.
(49) Soper, A. K. Empirical Potential Monte Carlo Simulation of Fluid Structure. *Chem. Phys.* **1996**, *202*, 295−306.
(50) Mark, P.; Nilsson, L. Structure and Dynamics of the TIP3P, SPC, and SPC/E Water Models at 298 K. *J. Phys. Chem. A* **2001**, *105*, 9954−9960.
(51) Laurent, H.; Soper, A. K.; Dougan, L. Trimethylamine N-Oxide (TMAO) Resists the Compression of Water Structure by Magnesium Perchlorate: Terrestrial Kosmotrope vs. Martian Chaotrope. *Phys. Chem. Chem. Phys.* **2020**, *22*, 4924−4937.
(52) Laurent, H.; Baker, D.; Soper, A.; Ries, M.; Dougan, L. Solute Specific Perturbations to Water Structure and Dynamics in Tertiary Aqueous Solution. *J. Phys. Chem. B* **2020**, *124*, 10983−10993.
(53) Imberti, S.; Botti, A.; Bruni, F.; Cappa, G.; Ricci, M. A.; Soper, A. K. Ions in Water: The Microscopic Structure of Concentrated Hydroxide Solutions. *J. Chem. Phys.* **2005**, *122*, No. 194509.
(54) Soper, A. K. The Radial Distribution Functions of Water as Derived from Radiation Total Scattering Experiments: Is There Anything We Can Say for Sure? *ISRN Phys. Chem.* **2013**, *2013*, No. 279463.
(55) Soper, A. K.; Ricci, M. A. Structures of High-Density and Low-Density Water. *Phys. Rev. Lett.* **2000**, *84*, 2881−2884.
(56) Soper, A. K. *Empirical Potential Structure Refinement: A User's Guide*; ISIS Neutron and Muon Facility, 2017.
(57) Rhys, N. H.; Soper, A. K.; Dougan, L. Hydrophilic Association in a Dilute Glutamine Solution Persists Independent of Increasing Temperature. *J. Phys. Chem. B* **2015**, *119*, 15644−15651.
(58) Mccune, J. A.; Turner, A. H.; Coleman, F.; White, C. M.; Callear, S. K.; Youngs, T. G. A.; Swadźba-Kwäny, M.; Holbrey, J. D. Association and Liquid Structure of Pyridine-Acetic Acid Mixtures Determined from Neutron Scattering Using a "free Proton" EPSR Simulation Model. *Phys. Chem. Chem. Phys.* **2015**, *17*, 6767−6777.
(59) Bowron, D. T.; Soper, A. K.; Finney, J. L. Temperature Dependence of the Structure of a 0.06 Mole Fraction Tertiary Butanol-Water Solution. *J. Chem. Phys.* **2001**, *114*, 6203−6219.
(60) Maugeri, L.; Busch, S.; McLain, S. E.; Pardo, L. C.; Bruni, F.; Ricci, M. A. Structure-Activity Relationships in Carbohydrates Revealed by Their Hydration. *Biochim. Biophys. Acta, Gen. Subj.* **2017**, *1861*, 1486−1493.
(61) Towey, J. J.; Soper, A. K.; Dougan, L. What Happens to the Structure of Water in Cryoprotectant Solutions? *Faraday Discuss.* **2013**, *167*, 159−176.
(62) Towey, J. J.; Barney, E. R. Multicomposition EPSR: Toward Transferable Potentials to Model Chalcogenide Glass Structures. *J. Phys. Chem. B* **2016**, *120*, 13169−13183.
(63) Norman, S. E.; Turner, A. H.; Youngs, T. G. A. Structure of Ionic Liquids with Amino Acid Anions via Neutron Diffraction. *RSC Adv.* **2015**, *5*, 67220−67226.
(64) Headen, T. F. Temperature Dependent Structural Changes in Liquid Benzene Studied Using Neutron Diffraction. *Mol. Phys.* **2019**, *117*, 3329−3336.
(65) Hore, P. J. *Nuclear Magnetic Resonance*, 2nd ed.; Oxford University Press: Oxford, 2014.
(66) Claridge, T. D. W. *High-Resolution NMR Techniques in Organic Chemistry*, 3rd ed.; Elsevier: Oxford, 2016.

https://doi.org/10.1021/acs.jpcb.1c06728
J. Phys. Chem. B 2021, 125, 12774−12786

(67) Lambert, J. B.; Mazzola, E. P. *Nuclear Magnetic Resonance Spectroscopy: An Introduction to Principles, Applications, and Experimental Methods*; Pearson Education, Inc.: Upper Saddle River, 2004.
(68) Stejskal, E. O.; Tanner, J. E. Spin Diffusion Measurements: Spin Echoes in the Presence of a Time-Dependent Field Gradient. *J. Chem. Phys.* **1965**, *42*, 288−292.
(69) Chieh, C. P. Hydration. https://chem.libretexts.org/Bookshelves/Physical_and_Theoretical_Chemistry_Textbook_Maps/Supplemental_Modules_(Physical_and_Theoretical_Chemistry)/Thermodynamics/Energies_and_Potentials/Enthalpy/Hydration (accessed Mar 18, 2021).
(70) Tissandier, M. D.; Cowen, K. A.; Feng, W. Y.; Gundlach, E.; Cohen, M. H.; Earhart, A. D.; Coe, J. V.; Tuttle, T. R. The Proton's Absolute Aqueous Enthalpy and Gibbs Free Energy of Solvation from Cluster-Ion Solvation Data. *J. Phys. Chem. A* **1998**, *102*, 7787−7794.
(71) Shannon, R. D. Revised Effective Ionic Radii and Systematic Studies of Interatomic Distances in Halides and Chalcogenides. *Acta Crystallogr., Sect. A* **1976**, *32*, 751−767.
(72) Laage, D.; Stirnemann, G. Effect of Ions on Water Dynamics in Dilute and Concentrated Aqueous Salt Solutions. *J. Phys. Chem. B* **2019**, *123*, 3312−3324.
(73) Jones, G.; Dole, M. The Viscosity of Aqueous Solutions of Strong Electrolytes with Special Reference to Barium Chloride. *J. Am. Chem. Soc.* **1929**, *51*, 2950−2964.
(74) Smith, D. W. Ionic Hydration Enthalpies. *J. Chem. Educ.* **1977**, *54*, 540−542.
(75) Zhang, Q.; Chen, H.; Wu, T.; Jin, T.; Pan, Z.; Zheng, J.; Gao, Y.; Zhuang, W. The Opposite Effects of Sodium and Potassium Cations on Water Dynamics. *Chem. Sci.* **2017**, *8*, 1429−1435.

https://doi.org/10.1021/acs.jpcb.1c06728
J. Phys. Chem. B 2021, 125, 12774−12786